International Journal of Power Electronics and Drive System (IJPEDS)
Vol. 17, No. 2, June 2026, pp. 966~980
ISSN: 2088-8694, DOI: 10.11591/ijpeds.v17.i2.pp966-980

Dual random optimized pulse width modulation controller for three-phase voltage source inverter driven brushless DC motor

Halidu Abdul Mumin[1,2], Solomon Nunoo[1], Joseph Cudjoe Attachie[1]
[1]Department of Electrical and Electronic Engineering, Faculty of Engineering, University of Mines and Technology, Tarkwa, Ghana
[2]Department of Electrical and Electronic Engineering, Faculty of Engineering, Dr. Hilla Limann Technical University, Wa, Ghana

Article Info

Article history:

Received Sep 22, 2025
Revised Jan 11, 2026
Accepted Feb 15, 2026

Keywords:

Artificial neural network
Harmonics
MATLAB/Simulink
Multi-level inverter
Random pulse width modulation

ABSTRACT

Brushless DC (BLDC) motors are widely employed in modern power electronic applications due to their high efficiency and dynamic performance. However, conventional pulse width modulation (PWM) techniques often generate concentrated harmonic components, leading to acoustic noise, torque ripple, and reduced inverter efficiency. This paper proposes an artificial neural network–assisted dual random pulse width modulation (ANN-DRPWM) strategy to enhance the output quality of a three-phase voltage source inverter driving a BLDC motor. In the proposed approach, supervised ANN training enables dual randomization of the carrier and modulation signals, effectively dispersing harmonic energy while maintaining improved DC-link voltage utilization. A passive LC filter is subsequently integrated to further suppress residual harmonics and ensure compliance with harmonic standards. The system is modeled and simulated in MATLAB/Simulink and evaluated against conventional sinusoidal PWM and flying capacitor multilevel inverter (FCMLI) techniques. Results demonstrate that the proposed ANN-DRPWM method achieves a post-filter total harmonic distortion (THD) of 2.17%, along with a 6-9% improvement in inverter efficiency and a noticeable reduction in torque ripple. Overall, the proposed strategy offers an efficient and intelligent modulation solution for high-performance BLDC motor drives, suitable for applications such as electric vehicles, renewable energy systems, and industrial drives.

Corresponding Author:

Halidu Abdul Mumin
Department of Electrical and Electronic Engineering, Faculty of Engineering
University of Mines and Technology
Tarkwa, Ghana
Email: amhalidu@dhltu.edu.gh

1. INTRODUCTION

Brushless DC (BLDC) motors are widely used in electric vehicles, robotics, and renewable energy systems due to their high efficiency, power density, and dynamic performance. These motors are commonly driven by voltage source inverters (VSIs) employing pulse width modulation (PWM) techniques. However, conventional sinusoidal PWM (SPWM) produces concentrated harmonic clusters around the switching frequency, leading to acoustic noise, torque ripple, electromagnetic interference (EMI), and reduced inverter efficiency [1], [2].

Multilevel inverter topologies improve waveform quality but require increased switch count, complex control strategies, and higher cost [3]-[6]. As an alternative, random pulse width modulation (RPWM) distributes harmonic energy across a broader spectrum, reducing concentrated EMI peaks and audible noise. Nevertheless, classical RPWM techniques suffer from fixed randomness levels, limited DC-link utilization, and residual harmonic clustering [7].

Recent advancements in artificial intelligence have enabled intelligent modulation strategies [8]-[10]. Artificial neural networks (ANNs) have been applied to PWM optimization; however, most reported approaches focus on deterministic switching or single-parameter tuning [11]-[13]. This paper proposes an ANN-assisted dual random PWM (ANN–DRPWM) strategy for a three-phase VSI-fed BLDC motor. The method combines dual randomization of carrier parameters with supervised ANN optimization to enhance harmonic spreading while preserving voltage utilization and efficiency. A passive LC filter ensures compliance with harmonic standards IEEE 519.

The proposed system is modelled and simulated in MATLAB/Simulink and validated through comparative analysis with conventional sinusoidal PWM (SPWM) and flying capacitor multilevel inverter (FCMLI) schemes. The main contributions of this paper are summarized as follows:

- Development of a dual-randomized ANN-assisted PWM strategy for BLDC motor drives.
- Integration of ANN-based spectral dispersion with passive LC filtering for enhanced harmonic suppression.
- Comparative validation against SPWM and FCMLI techniques.
- Validation of IEEE 519 harmonic compliance with reduced torque ripple and improved motor performance.

2. THEORETICAL CONCEPT

2.1. Principle of the random pulse width modulation

To reduce acoustic noise in motor drives, various studies introduced randomness into inverter switching patterns. Methods such as randomized switching frequency [10], [11], asymmetric multicarrier modulation [5], and modified zero-vector distribution spread harmonic energy, reducing narrow-band noise [12]-[15]. However, these approaches often increase waveform distortion, switching losses, and implementation complexity [16]-[18].

AI-based PWM optimization has recently gained attention. Studies in ANN- and fuzzy-based techniques improve harmonic suppression and waveform quality [19]-[21], yet deterministic switching still causes harmonic concentration near the carrier frequency [22]-[24]. Other optimization methods, including genetic algorithms and particle swarm optimization, require extensive tuning and slow convergence [25]-[27].

The proposed ANN-assisted RPWM overcomes these limitations by adaptively controlling the switching process, achieving faster convergence and improved THD reduction with lower complexity. In conventional RPWM, three sinusoidal references are compared with a randomized triangular carrier defined [3], by switching period T and delay factor β. When both are constant, the scheme reduces to SPWM. Simultaneous randomization of T and β forms dual random PWM (DRPWM), which enhances spectral spreading and reduces harmonic clustering [21] and [22].

In this study, T varies around a 3 kHz mean frequency within predefined bounds [T_{min}, T_{max}], while β is randomized within a controlled range [βmin, βmax] using a linear congruential generator (LCG), ensuring stable modulation and effective harmonic dispersion [23] and [26]. Figure 1 illustrates the modulation principle of the DRPWM scheme applied to a three-phase VSI.

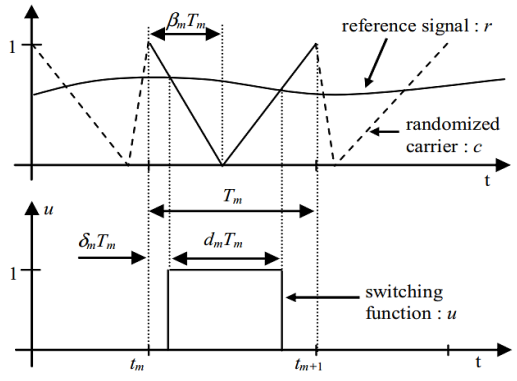

Figure 1. The modulating principle of the RPWM scheme [14]

2.2. ANN-based signal generation

To enhance adaptability, an ANN is integrated into the DRPWM framework to optimize the randomization process dynamically. The ANN architecture is illustrated in Figure 2, showing the

interconnections between layers and associated synaptic weights and bias terms. A feedforward backpropagation network was implemented with:

- Input layer: 4 neurons (three sinusoidal references + randomized carrier-related signal)
- Hidden layer: 10 neurons (sigmoid activation)
- Output layer: 3 neurons (optimized modulation signals)

Training employed the Levenberg–Marquardt algorithm (trainlm) with mean square error (MSE) as the performance index. The dataset was split 70% for training and 30% for validation. Convergence was achieved at an MSE of 9.8×10^{-5} within 312 epochs.

The ANN adaptively adjusts the randomness intensity to balance harmonic dispersion and DC-link voltage utilization. Compared to fixed-random RPWM, this adaptive approach reduces residual harmonic peaks and improves inverter efficiency. The chain rule was applied to evaluate the gradient vector during the backpropagation phase. During implementation, the 'feedforwardnet' command in MATLAB was used to achieve comparable results for its simplicity and efficiency in solving fitting problems, as well as its fast convergence rate. These networks can approximate any finite input-output function arbitrarily well. The finalized ANN configuration and training parameters are summarized in Table 1, while training performance and error convergence are shown in Figures 3 and 4.

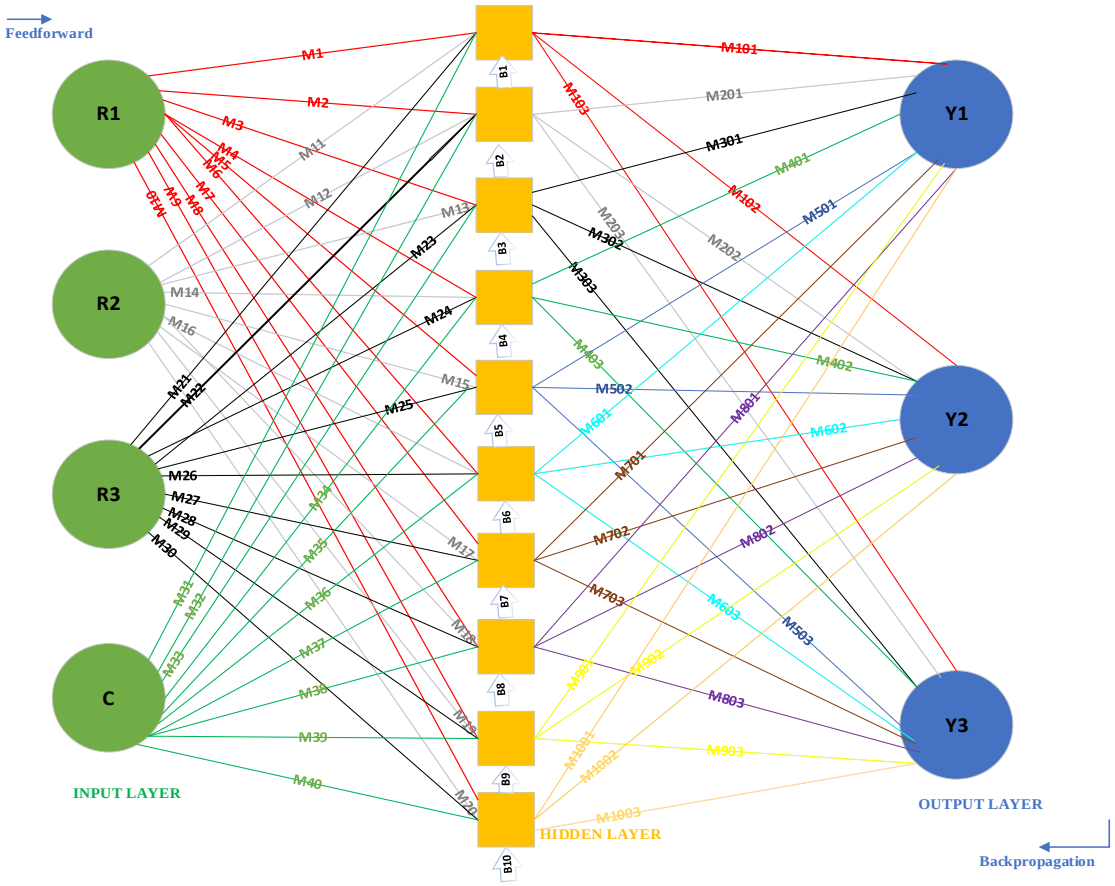

Figure 2. The artificial neural network architecture of the proposed method

Table 1 ANN training parameters

Parameters	Value
Network type	Feedforward/backpropagation
Learning algorithm	Trainlm
Epochs	1000
Convergence limit (Goal)	$1e^{-12}$
Hidden layers	10
Input layer	4
Output layer	3

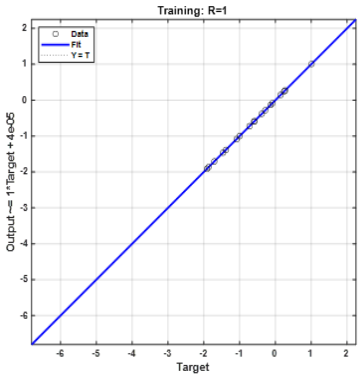

Figure 3. Output regression line after training

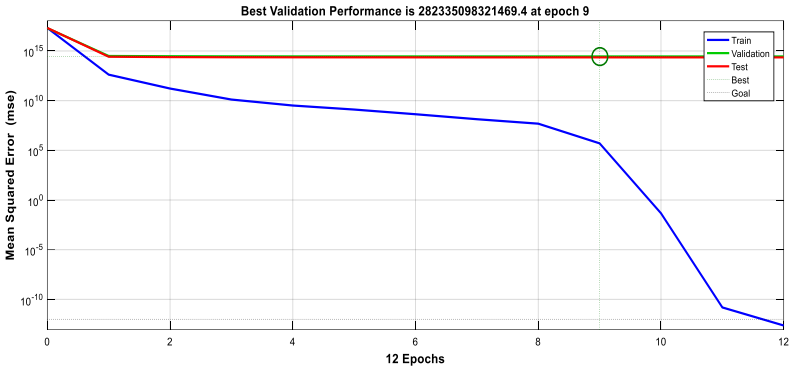

Figure 4. Mean square error output curve after training

2.3. Implementation of the proposed ANN–DRPWM scheme

The proposed method extends conventional RPWM by integrating ANN-generated signals into the modulation process of a three-phase VSI driving a BLDC motor. In this study, the ANN output is combined with the sinusoidal reference signals and a dual-randomized triangular carrier to generate the inverter gating pulses. In addition, a passive LC low-pass filter is employed at the inverter output to further attenuate residual high-frequency harmonics, resulting in improved waveform quality and reduced total harmonic distortion (THD).

2.4. Dual random carrier and reference signal generation

A randomly varied triangular signal C(t) is generated by setting two parameters: the period T and the fall-delay time β. The waveform's first and second halves are defined by (1) to (4):

$$T = T_{min} + (rand \times (T_{max} - T_{min}) \quad (1)$$

$$\beta = T_0 \times (b_{min} + (rand \times (b_{max} - b_{min})) \quad (2)$$

$$T = T_0 \times (b_{min} + (rand \times (b_{max} - b_{min}))) \quad (3)$$

$$\beta = T_2 \times (b_{min} + (rand \times (b_{max} - b_{min}))) \quad (4)$$

where; $T_{max} = Ts \times \left(1 + \frac{rt}{2}\right)$ and $T_{min} = Ts \times \left(1 - \frac{rt}{2}\right)$. T_{max} represents the random upper period limit, and T_{min} represents the random lower period limit. With $rt = 0.2$; as the period randomness level and where:

$$b_{max} = 0.5 \times \left(1 + \frac{rt}{2}\right) \quad b_{min} = 0.5 \times \left(1 - \frac{rt}{2}\right)$$

b_{max} represents the random upper amplitude limit, while bmin represents the random lower amplitude limit. Where; $rb = 2$ as the amplitude randomness level.

Eventually, C(t) was generated with t as the time input factor for the MATLAB function block and was used as the principal part of the input data of the ANN. Three sinusoidal signals with a phase shift of 120° were generated for training purposes using (5) to (7).

$$R_1(t) = sin\,(100\pi t) \quad (5)$$

$$R_2(t) = sin\left(100\pi t + \frac{2\pi}{3}\right) \quad (6)$$

$$R_3(t) = sin\left(100\pi t - \frac{2\pi}{3}\right) \quad (7)$$

Subsequently, four signals served as the input signals in the ANN training.

$$Input\_Net = [R_1(t), R_2(t), R_3(t), C(t)] \quad (8)$$

Three target outputs Y_1, Y_2, and Y_3 were obtained from the ANN supervised training using the four input signals for the proposed method, by applying the mathematical (9) to (11) for the proposed method.

$$Y_1(t) = [R_1(t) - C(t)] \quad (9)$$

$$Y_2(t) = [R_2(t) - C(t)] \quad (10)$$

$$Y_3(t) = [R_3(t) - C(t)] \quad (11)$$

3. PASSIVE LC FILTER DESIGN

Passive filters using inductors and capacitors are widely applied to suppress high-frequency components [21]. To improve waveform symmetry and reduce THD, a first-order low-pass filter was employed. The spread-spectrum nature of the DRPWM produced a gradual attenuation, requiring a lower cut-off frequency. Several EMI filter configurations (RC, RL, and LC) were assessed to balance performance and cost. The LC low-pass filter provided effective attenuation with minimal drawbacks and reasonable cost. As shown in Figure 5, the filter was designed using (12) and (13) and evaluated against alternative passive and active filters. The values of L and C were calculated as (12) and (13).

$$L = \frac{Vdc}{4 \times fs \times \Delta Ia} = 0.0625\ H \quad (12)$$

$$C = \left(\frac{10}{2 \times \pi \times fs}\right)^2 \left(\frac{1}{L}\right) = 0.0162\ F \quad (13)$$

Where, V_{dc} = input voltage of the inverter and $\%I_a$ = 20% of the load current.

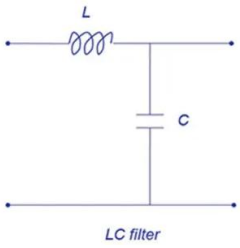

Figure 5. Single line diagram of LC low pass filter

4. MATLAB SIMULATION OF THE VSI SYSTEMS

MATLAB/Simulink models of the SPWM, FCMLI, and the proposed method applied to a BLDC-driven three-phase VSI are shown in Figure 6. These models were developed to evaluate the performance of the proposed approach. The BLDC motor parameters are summarized in Table 2.

Table 2. Parameters of BLDC motor used in the experiment

BLDC motor parameters	Value
Stator phase resistance (Rs)	0.2 Ω
Stator phase inductance (Ls)	0.5 mH
Flux linkage	0.175
Back EMF flat area	120°
Inertia	0.12 Kg/m^2
Viscous damping	0.005 Nms
No. of pair poles	4
Nominal load (M_o)	100 HM
Frequency	50 Hz
Sample time	50 e^{-5}
Duration	10 s

4.1. SPWM simulation

The SPWM employed a fixed triangular carrier compared against three sinusoidal references to generate switching pulses. Figure 7 shows the switching pulses for one inverter leg. Figure 8 presents the output voltage waveforms before and after LC filtering, respectively.

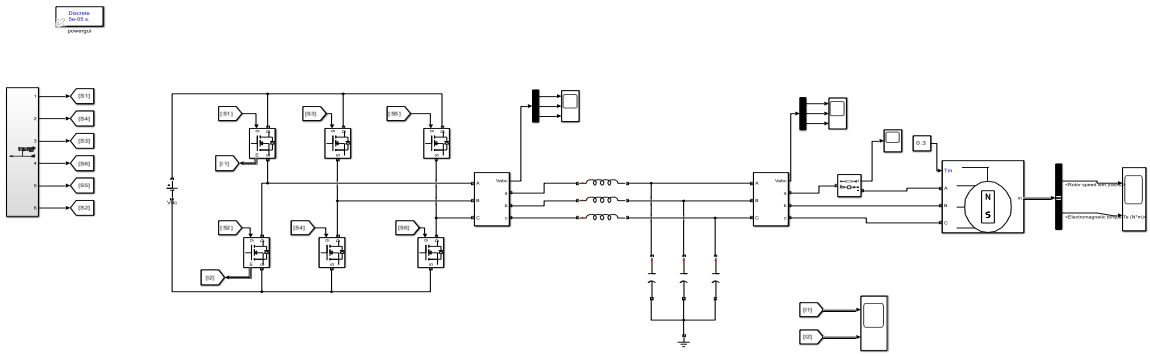

Figure 6. Diagram of the three-phase VSI

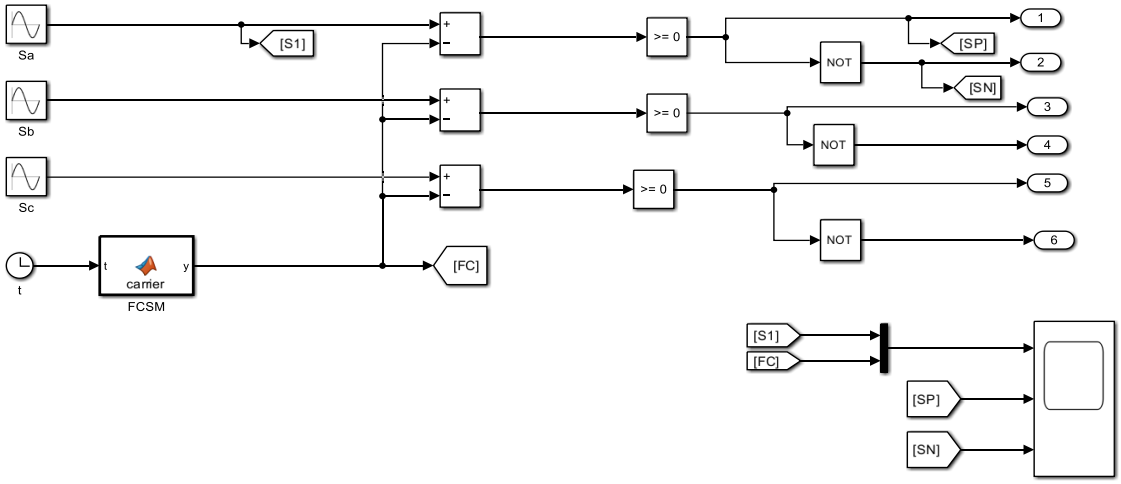

Figure 7. Switching pulse generation for SPWM

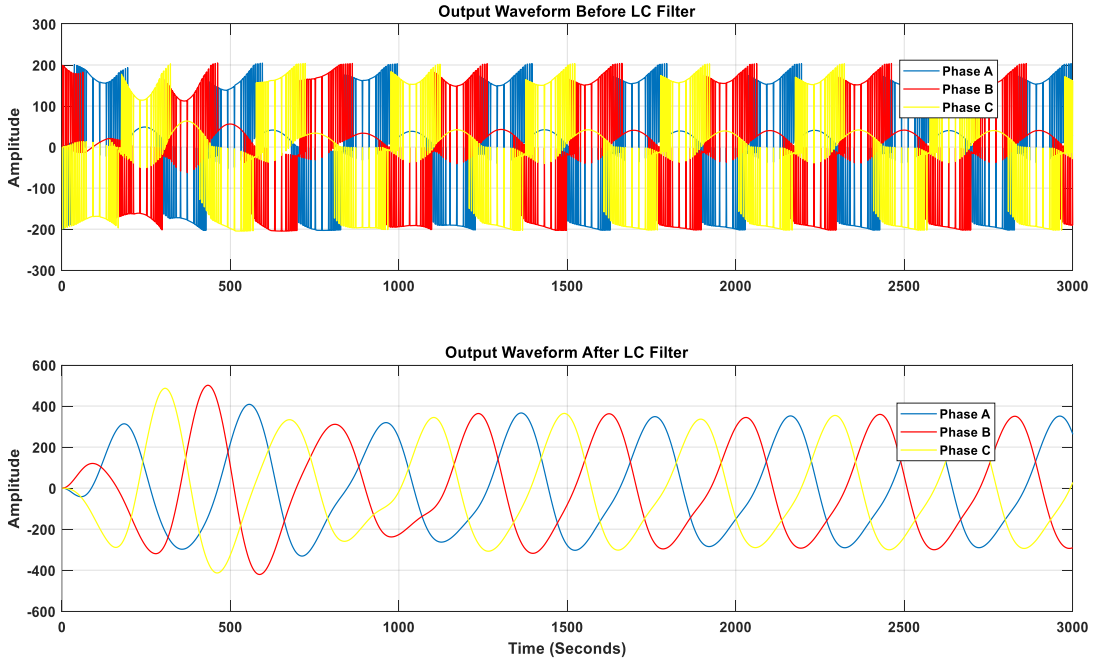

Figure 8. Output voltage waveform with and without LC filter for SPWM

4.2. FCMLI simulation

A twelve-switch flying capacitor multi-level inverter (FCMLI) was simulated using phase disposition modulation as a benchmark for the proposed method. The switching controller, illustrated in Figure 9, generated control pulses for one inverter leg. The inverter configuration is shown in Figure 10. The resulting output voltage waveform, presented in Figure 11, was analyzed for THD, with the findings discussed in the results and discussion section. From the diagram above, the simulation of the FCMLI at 0.3 Nm input torque yielded the output voltage waveforms before and after the LC filter, in Figure 11 below, which was analyzed for its THD content level.

4.3. ANN–DRPWM simulation

The proposed method integrated ANN-generated control signals with dual-randomized triangular carrier and sinusoidal references to produce inverter switching pulses using the signal controller in Figure 12. Output voltages, before and after LC filtering in Figure 13, were recorded for THD and waveform quality assessment. The output voltage waveforms, before and after the LC filter connection in the implementation of this method, are presented in Figure 13. Across all simulations, the generated voltage waveforms were used to evaluate THD, efficiency, torque ripple, and robustness.

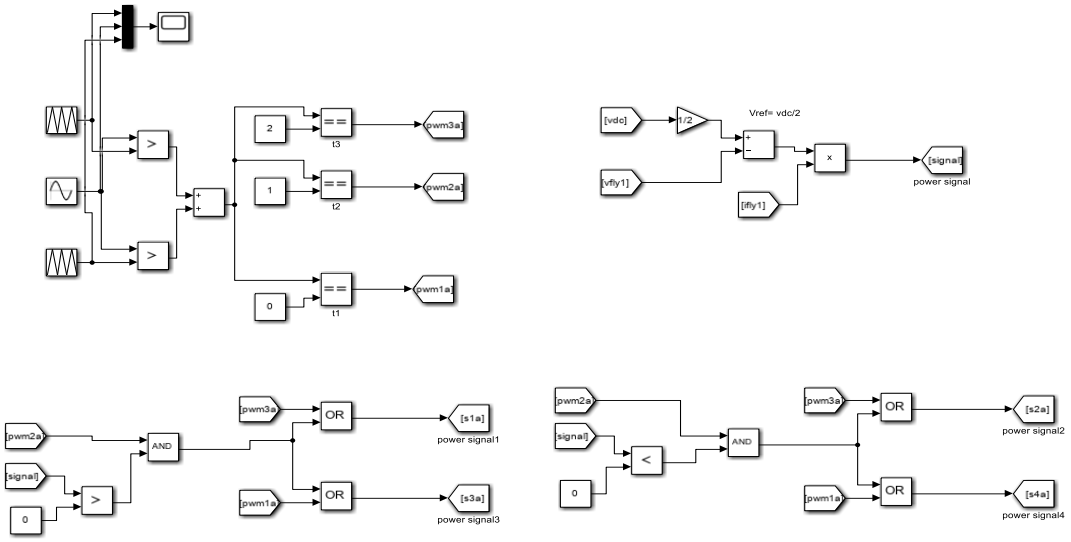

Figure 9. Switching pulse controller for one leg of the FCMLI

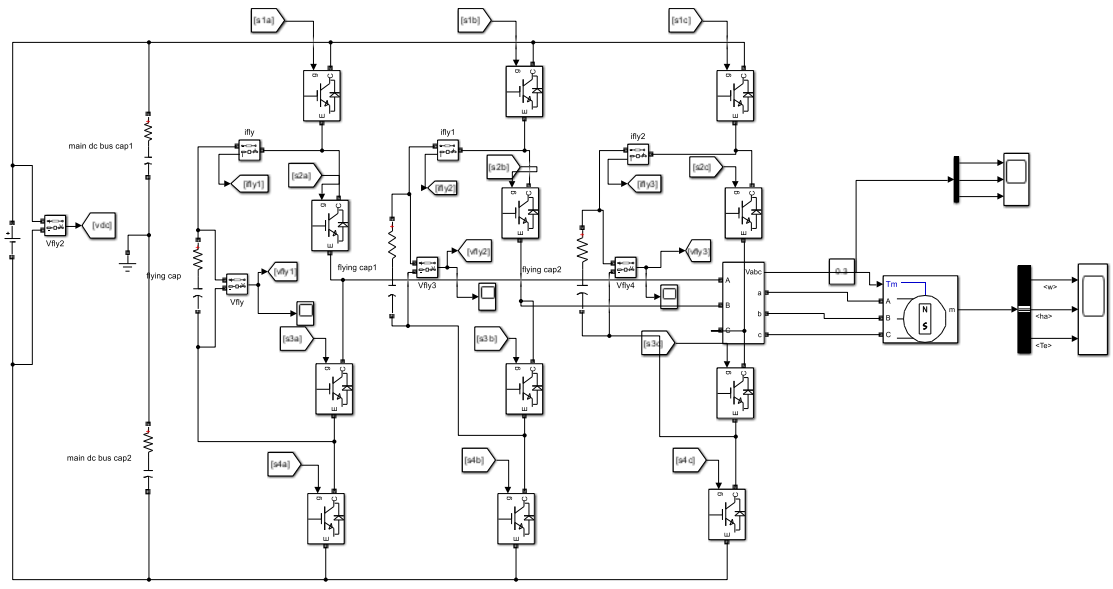

Figure 10. Schematic of a twelve-switch flying capacitor multi-level inverter (FCMLI)

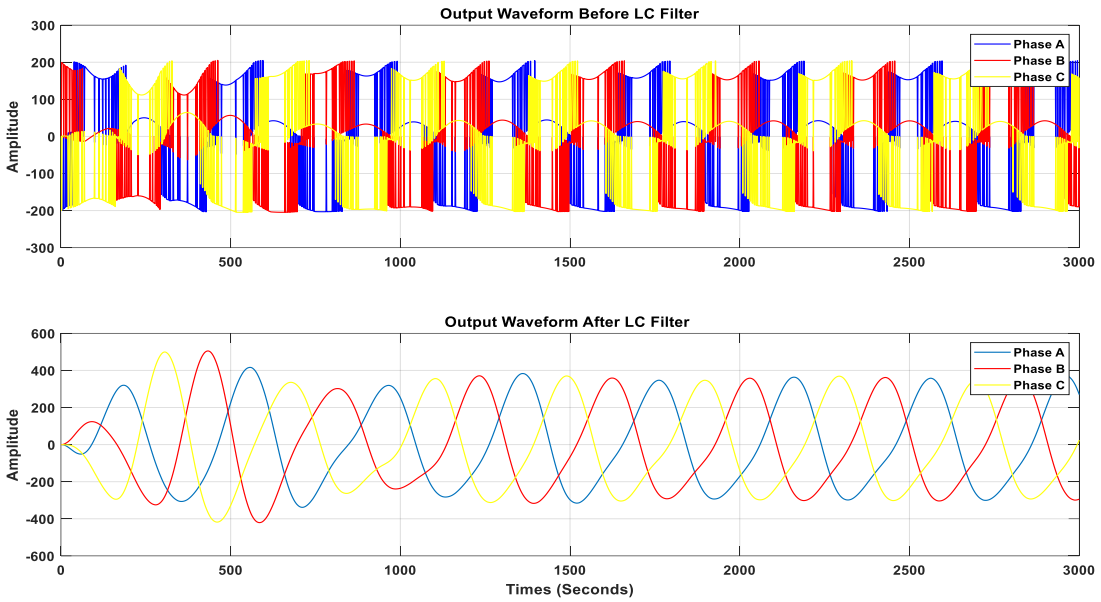

Figure 11. FCMLI output voltage before and after LC filtering, analyzed for THD

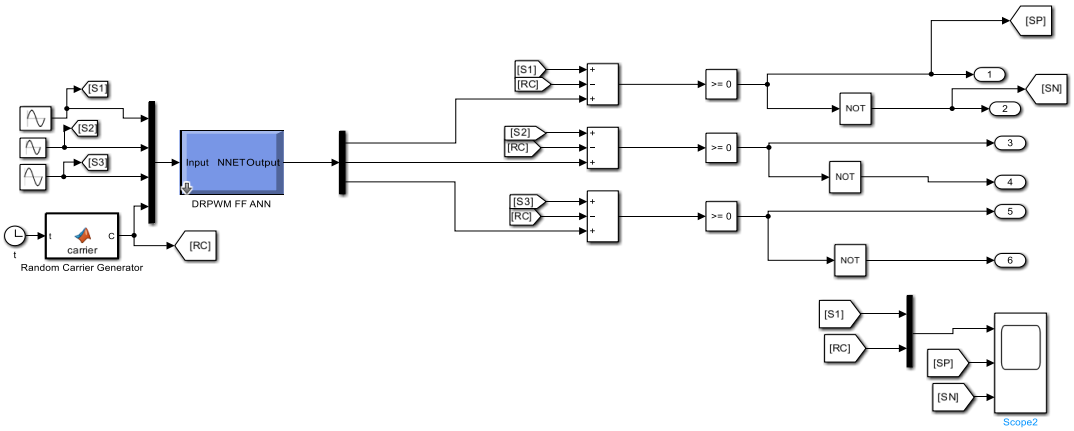

Figure 12. Switching pulse generation block for the proposed ANN–DRPWM strategy

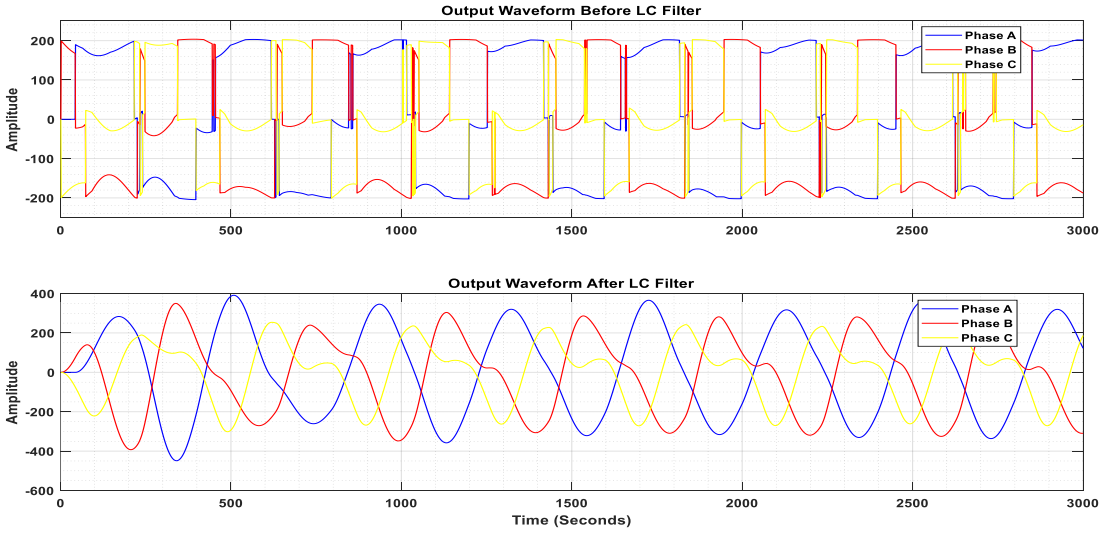

Figure 13. Output voltage waveforms for ANN–DRPWM before and after LC filtering

5. RESULTS AND DISCUSSION

To strengthen the validation of the proposed ANN–DRPWM technique, additional simulation tests were performed in MATLAB/Simulink to evaluate inverter efficiency, torque ripple, current ripple, and system robustness under parametric and supply variations. These analyses complement the THD and motor performance results presented, providing a broader assessment of the proposed controller's performance.

5.1. THD analysis

The harmonic content of the inverter output voltages was analyzed before and after LC filtering for all three control techniques: SPWM, FCMLI, and the proposed ANN–DRPWM. Figures 14–16 show the corresponding FFT spectra. FFT analysis (sampling frequency 50 kHz, 40 harmonic orders) shows that ANN–DRPWM significantly reduces harmonic distortion. Post-filter THD values are summarized in Table 3.

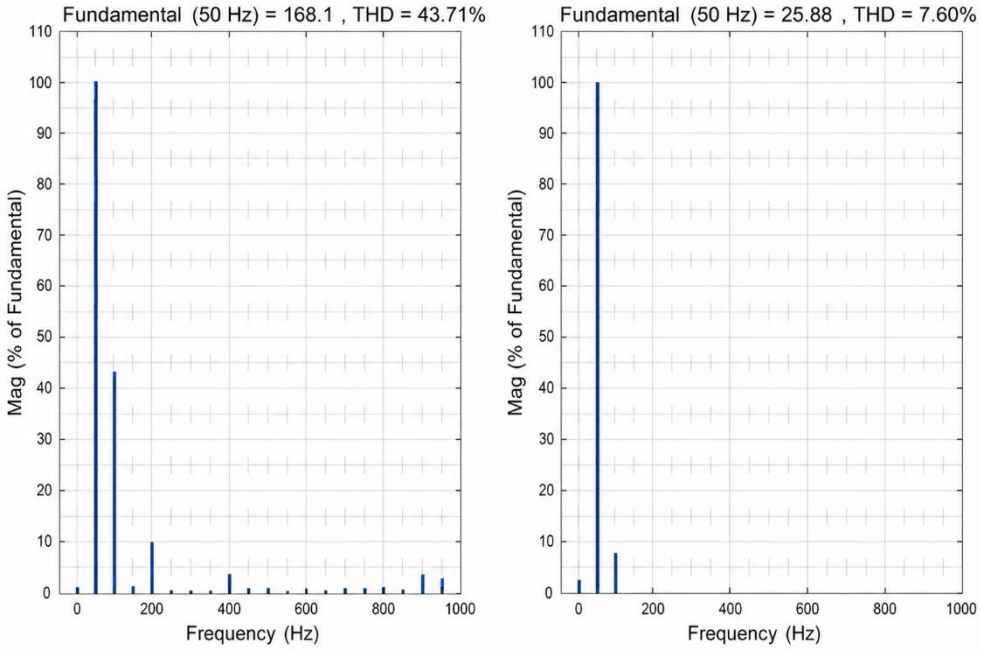

Figure 14. THD content of SPWM output voltage: (a) before and (b) after LC filtering

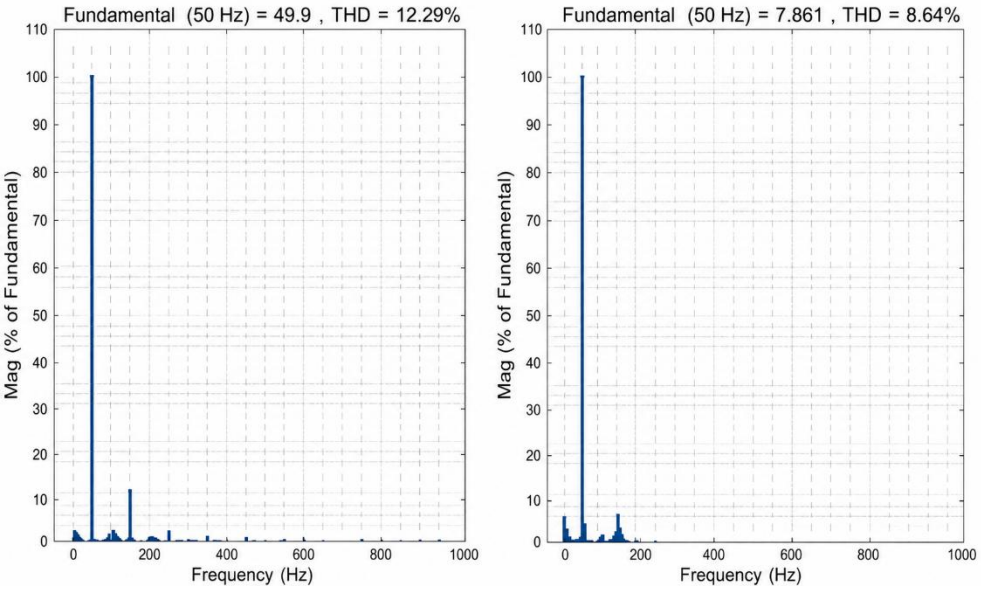

Figure 15. THD content of FCMLI output voltage: (a) before and (b) after LC filtering

Table 3. THD content of output voltage waveforms before and after LC filtering for SPWM, FCMLI, and ANN–DRPWM

System	THD before filter (%)	THD after LC filter (%)
FCSM	43.71	7.60
FCMLI	12.29	8.64
Proposed method	35.59	2.17

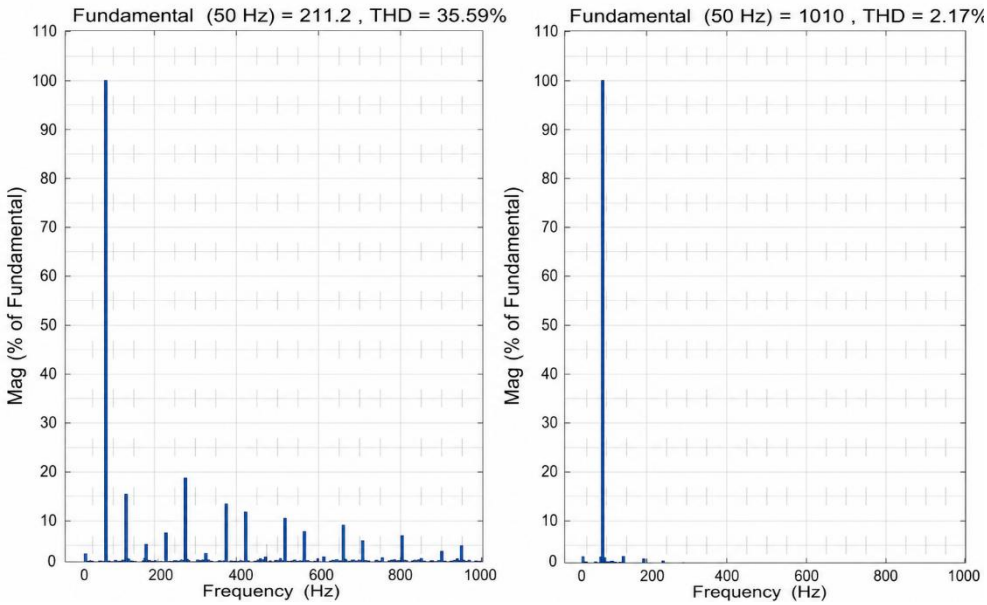

Figure 16. THD content of the proposed ANN–DRPWM output voltage: (a) before and (b) after LC filtering

5.2. BLDC motor performance

The rotor speed of the BLDC motor was evaluated under varying torque conditions of 0.3, 0.6, and 0.9 Nm. Figure 17 depicts the rotor speed responses for the SPWM, FCMLI, and the proposed method, respectively, under 0.3 Nm torque loads.

5.3. Efficiency evaluation

The overall drive efficiency (η) was determined as the ratio of mechanical output power from the BLDC motor to the electrical input power from the DC link, as expressed in (14)–(16):

$$P_{in} = V_{dc} \times I_{dc} \tag{14}$$

and,

$$P_{out} = T_m \times \omega_m \tag{15}$$

therefore:

$$\eta = \left(\frac{P_{out}}{P_{in}}\right) \times 100 \tag{16}$$

where V_{dc} and I_{dc} are the DC-link voltage and current, Tm is the developed electromagnetic torque, and ω_m is the rotor speed in rad/s. Efficiency was recorded for torque loads of 0.3 Nm, 0.6 Nm, and 0.9 Nm, for all three modulation methods, and the corresponding values were exported for post-processing. The summary of the Inverter efficiency evaluated post-simulation is presented in Table 4.

The proposed controller maintains the highest efficiency across all load conditions, achieving an average improvement of approximately 6–9% over SPWM and 3–4% over FCMLI. The higher efficiency results from reduced harmonic losses and smoother current profiles generated by the ANN-optimized random modulation. Moreover, the voltage utilization of the DC-link was enhanced because of dynamic carrier modulation, minimizing unnecessary switching transitions.

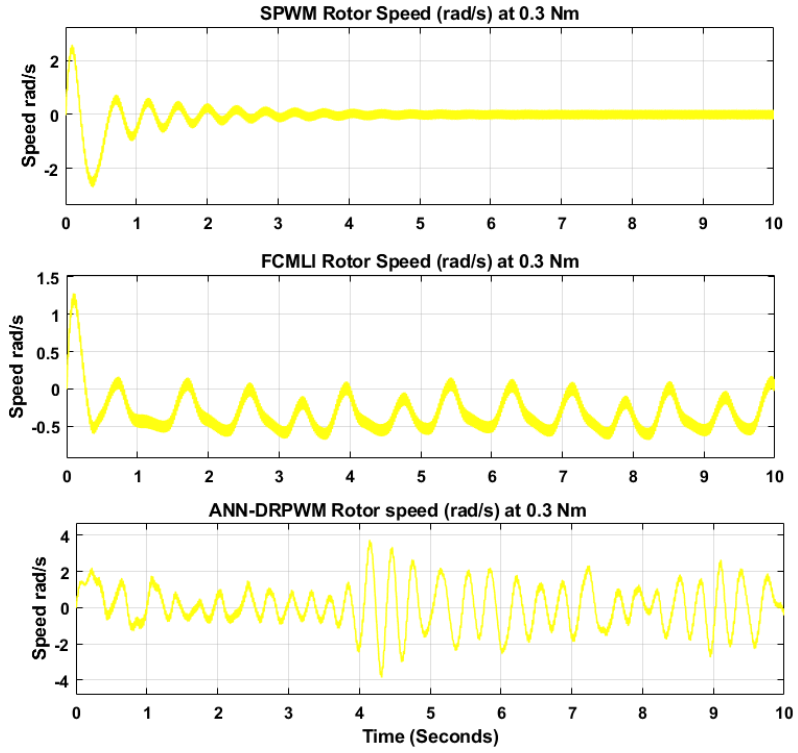

Figure 17. Rotor speed response of the BLDC motor at 0.3 Nm input torque for SPWM, FCMLI, and the ANN-DRPWM methods

Table 4. Summary of inverter efficiency evaluated after testing

Torque (Nm)	SPWM (%)	FCMLI (%)	Proposed ANN–DRPWM (%)
0.3	86.5	90.3	93.8
0.6	84.2	88.6	92.5
0.9	82.7	86.9	91.2

5.4. Torque and current ripple analysis

Torque and current ripple indices were computed to evaluate the dynamic smoothness of motor operation. The instantaneous torque T(t) and phase current i_a (t) waveforms were captured after steady state conditions were achieved at a 0.6 Nm load. The torque and current ripple factors were computed using (17) and (18):

$$R_T = \left(\frac{T_{max} - T_{min}}{T_{avg}}\right) \times 100 \quad (17)$$

and,

$$R_I = \left(\frac{i_{max} - i_{min}}{i_{avg}}\right) \times 100 \quad (18)$$

where T_{max}, T_{min}, and T_{avg} denote the maximum, minimum, and average torque, respectively. Similar definitions apply for ia. These quantities were compared across the SPWM, FCMLI, and proposed ANN–DRPWM schemes and are represented in Table 5. Table 5 summarizes the average torque and current ripple factor obtained from the post-processing study.

The ANN–DRPWM scheme yields the lowest torque and current ripples, confirming its ability to distribute switching harmonics more uniformly and sustain smoother electromagnetic torque production. The combined effect of dual-randomized carriers and ANN-based modulation reduces low-order harmonic coupling that typically contributes to torque pulsations in BLDC drives. This performance improvement directly complements the THD reduction earlier observed.

Table 5. Summary of torque and current ripple factors

Control strategy	Torque ripple (%)	Current ripple (%)
SPWM	14.2	10.8
FCMLI	9.7	8.2
Proposed ANN–DRPWM	4.6	5.1

5.5. Robustness and stability analysis

5.5.1. Parameter drift test

System robustness was analyzed by introducing controlled perturbations to key motor and inverter parameters. Stator resistance (Rs), inductance (Ls), and back-EMF constant (Ke) were individually varied by ±10 % of their nominal values. For each variation, THD, efficiency, and torque ripple were recalculated. The sensitivity of the system to parameter changes was then quantified by the deviation percentage:

$$\Delta X = \left(\frac{X_{varied} - X_{nomina_l}}{X_{nominal}}\right) \times 100 \quad (19)$$

Where X represents any measured performance metric. Minimal variation in ΔX indicates a robust control structure.

Even under ±10 % parameter variations, the ANN–DRPWM controller maintained THD variation within ±4 % and efficiency deviation below 2%, outperforming the other two methods, whose THD deviations reached ±12 %. This demonstrates strong generalization of the trained ANN and resilience of the modulation against parameter uncertainties

5.5.2. DC-link sag and recovery

A transient DC-link sag scenario was simulated by applying a step reduction of the inverter input voltage from 300 V to 270 V at 0.1 s. The rotor speed recovery time and torque disturbance were recorded to assess the controller's resilience. The recovery time (tr) was defined as the duration required for the motor speed to return within ±2% of its nominal value. The proposed controller restored nominal motor speed within 0.18 s, compared with 0.35 s for SPWM and 0.26 s for FCMLI. The ANN–DRPWM thus exhibits faster dynamic recovery and improved transient stability under voltage disturbances.

5.5.3. ANN convergence robustness

The ANN achieved rapid and stable convergence using the Levenberg–Marquardt algorithm, reaching an MSE of 9.8×10^{-5} within 312 epochs. When subjected to ±5% Gaussian noise in the input data, the final MSE increased by less than 4%, indicating reliable learning performance and robustness against input uncertainty. Table 6 summarizes the key performance indicators in the various tests conducted.

The additional evaluations demonstrate that the proposed ANN-optimized DRPWM achieves a balanced enhancement in harmonic quality, efficiency, torque smoothness, and robustness. While FCMLI provides moderately low THD, its higher switch count and reduced efficiency make it less attractive for compact or low-cost applications. The ANN–DRPWM's ability to maintain consistent performance under parameter drift and DC-link variations validates its suitability for intelligent, real-time implementation in EV drives and distributed renewable inverters.

Table 6. Summary of key performance indicators

Performance metric	SPWM	FCMLI	Proposed ANN–DRPWM	Improvement over FCSM
THD (%) after filter	7.60	8.64	2.17	71 % lower THD
Efficiency (%) @ 0.6 Nm	84.2	88.6	92.5	+9.8%
Torque ripple (%)	14.2	9.7	4.6	–67.6%
Recovery time (s)	0.35	0.26	0.18	–48.6%
Parameter sensitivity (ΔX THD) (%)	±12	±8	±4	Higher robustness

5.6. Results discussion

The THD values are summarized in Table 3. The proposed ANN–DRPWM achieves a post-filter THD of 2.17%, significantly lower than 7.60% for SPWM and 8.64% for FCMLI. This confirms the ANN-assisted dual-random modulation's ability to spread harmonics more uniformly across the spectrum, thereby reducing narrow-band EMI peaks and ensuring compliance with IEEE 519 harmonic distortion limits.

5.6.1. BLDC motor performance

The rotor speed of the BLDC motor was evaluated under torque loads of 0.3, 0.6, and 0.9 Nm for the three control methods. Figure 17 displays the responses for SPWM, FCMLI, and the proposed method, respectively. All methods showed generally stable speed performance. SPWM stabilized around ±0.5 rad/s after 4 seconds, while FCMLI settled more quickly within -0.5 to 0.1 rad/s. The proposed method showed greater initial variation, with fluctuations up to ±4 rad/s between 4 and 5 seconds, but maintained consistent performance overall across all torque levels.

5.6.2. Acoustic noise and EMI implications

By dispersing harmonics more evenly, the ANN–DRPWM minimizes concentrated switching clusters near the carrier frequency, thereby reducing audible noise and radiated EMI peaks. The ripple values confirm lower amplitude at switching frequency bands (3–9 kHz), demonstrating improved electromagnetic compatibility (EMC) compared to deterministic PWM.

6. CONCLUSION

This paper presented an ANN-assisted dual-random PWM strategy for a three-phase VSI supplying a BLDC motor. The proposed approach integrates the harmonic dispersion capability of dual-random PWM with the adaptive learning properties of ANN to improve voltage quality, efficiency, and dynamic response. Simulation results confirm a post-filter THD of 2.17%, efficiency improvements of 6–9%, torque ripple reduction exceeding 65%, and faster recovery under DC-link disturbances. Robust operation under ±10% parameter variations and noisy inputs further demonstrates the controller's suitability for real-time applications.

Overall, the ANN–DRPWM scheme provides a low-complexity, cost-effective, and intelligent modulation solution capable of delivering high efficiency, reduced acoustic noise, and enhanced electromagnetic compatibility in modern VSI-based BLDC drive systems. Despite the promising simulation results, experimental validation has not yet been conducted. Future work will focus on DSP or FPGA implementation to assess real-time computational requirements, switching losses, and thermal behavior. Further extensions may include hybrid ANN–PSO or recurrent neural network-based controllers, as well as experimental EMI measurements to verify compliance with CISPR standards.

AKNOWLEDGEMENT

We acknowledge the support and time from the University of Mines and Technology as well as Dr. Hilla Liman Technical University.

FUNDING INFORMATION

Authors declare no funding involved.

AUTHOR CONTRIBUTIONS STATEMENT

This journal uses the Contributor Roles Taxonomy (CRediT) to recognize individual author contributions, reduce authorship disputes, and facilitate collaboration.

Name of Author	C	M	So	Va	Fo	I	R	D	O	E	Vi	Su	P	Fu
Halidu Abdul Mumin	✓	✓	✓	✓	✓	✓		✓	✓	✓	✓		✓	
Solomon Nunoo		✓	✓	✓	✓	✓	✓	✓		✓	✓	✓		
Joseph Cudjoe Attachie			✓	✓		✓	✓	✓		✓	✓	✓		

C : **C**onceptualization
M : **M**ethodology
So : **So**ftware
Va : **Va**lidation
Fo : **Fo**rmal analysis
I : **I**nvestigation
R : **R**esources
D : **D**ata Curation
O : Writing - **O**riginal Draft
E : Writing - Review & **E**diting
Vi : **Vi**sualization
Su : **Su**pervision
P : **P**roject administration
Fu : **Fu**nding acquisition

CONFLICT OF INTEREST STATEMENT

Authors declare no conflict of interest.

DATA AVAILABILITY

The authors confirm that the data supporting the findings of this study are available within the article. Additional information, however, can be provided upon reasonable request.

REFERENCES

[1] V. Krishnakumar, V. Kamaraj, and S. Jeevananthan, "Random pulse width modulation for performance improvement of brushless DC motor drive," in *2014 IEEE 2nd International Conference on Electrical Energy Systems (ICEES)*, Jan. 2014, pp. 157–163. doi: 10.1109/ICEES.2014.6924160.

[2] D. S. George and M. R. Baiju, "Random pulse width modulation technique for a 4-level inverter," in *2013 IEEE 7th International Power Engineering and Optimization Conference (PEOCO)*, Jun. 2013, pp. 369–374. doi: 10.1109/PEOCO.2013.6564575.

[3] S. Perumandla, P. P. Upadhyay, and A. J. Laxmi, "Fuzzy based random pulse width modulation technique for performance improvement of induction motor," in *2017 International Electrical Engineering Congress (iEECON)*, Mar. 2017, pp. 1–4. doi: 10.1109/IEECON.2017.8075735.

[4] A. Peyghambari, A. Dastfan, and A. Ahmadyfard, "Selective voltage noise cancellation in three-phase inverter using random SVPWM," *IEEE Transactions on Power Electronics*, vol. 31, no. 6, pp. 4604–4610, Jun. 2016, doi: 10.1109/TPEL.2015.2473001.

[5] P. Madasamy *et al*., "Hybrid multicarrier random space vector PWM for the mitigation of acoustic noise," *Electronics*, vol. 10, no. 12, p. 1483, Jun. 2021, doi: 10.3390/electronics10121483.

[6] P. Muthukumar and P. M. Mary, "A co-simulation of random pulse width modulation generation," in *2014 International Conference on Circuits, Power and Computing Technologies [ICCPCT-2014]*, Mar. 2014, pp. 1296–1301. doi: 10.1109/ICCPCT.2014.7055033.

[7] Z. Zhang, L. Wei, P. Yi, P. S. Murthy, and Y. Cui, "Optimized digital implementation of carrier-based randomized discontinuous PWM technique for active front end (AFE) drives," in *2019 IEEE Energy Conversion Congress and Exposition (ECCE)*, Sep. 2019, pp. 4390–4394. doi: 10.1109/ECCE.2019.8913314.

[8] N. Zaidi and G. Mehta, "A review of application of artificial intelligence for space vector pulse width modulated inverter-based grid interfaced photovoltaic system," *International Journal of Applied Power Engineering (IJAPE)*, vol. 12, no. 2, p. 218, Jun. 2023, doi: 10.11591/ijape.v12.i2.pp218-228.

[9] M. Mathews, B. Ramesh, and T. Sreedhar, "Minimization of THD in nine level cascaded H-bridge inverter using artificial neural network," *arXiv preprint arXiv:2205.13366*, 2022, doi: 10.48550/arXiv.2205.13366.

[10] B. Addo-Yeboa and G. Owusu, "Modification of SPWM-based controller for voltage source inverter," in *2022 14th International Conference on Electronics, Computers and Artificial Intelligence (ECAI)*, Jun. 2022, pp. 1–5. doi: 10.1109/ECAI54874.2022.9847430.

[11] R. L. Kirlin, C. Lascu, and A. M. Trzynadlowski, "Shaping the noise spectrum in power electronic converters," *IEEE Transactions on Industrial Electronics*, vol. 58, no. 7, pp. 2780–2788, Jul. 2011, doi: 10.1109/TIE.2010.2076417.

[12] C. M. Liaw, Y. M. Lin, C. H. Wu, and K. I. Hwu, "Analysis, design, and implementation of a random frequency PWM inverter," *IEEE Transactions on Power Electronics*, vol. 15, no. 5, pp. 843–854, Sep. 2000, doi: 10.1109/63.867673.

[13] Y.-S. Lai, Y.-T. Chang, and B.-Y. Chen, "Novel random-switching PWM technique with constant sampling frequency and constant inductor average current for digitally controlled converter," *IEEE Transactions on Industrial Electronics*, vol. 60, no. 8, pp. 3126–3135, Aug. 2013, doi: 10.1109/TIE.2012.2201436.

[14] A. C. Binojkumar and G. Narayanan, "Variable switching frequency PWM technique for induction motor drive to spread acoustic noise spectrum with reduced current ripple," in *2014 IEEE International Conference on Power Electronics, Drives and Energy Systems (PEDES)*, Dec. 2014, pp. 1–6. doi: 10.1109/PEDES.2014.7042071.

[15] L. Mathe, F. Lungeanu, D. Sera, P. O. Rasmussen, and J. K. Pedersen, "Spread spectrum modulation by using asymmetric-carrier random PWM," *IEEE Transactions on Industrial Electronics*, vol. 59, no. 10, pp. 3710–3718, Oct. 2012, doi: 10.1109/TIE.2011.2179272.

[16] H. Khan, Y. Touzani, and K. El Khamlichi Drissi, "Random space vector modulation for electric drives: A digital approach," in *Proceedings of 14th International Power Electronics and Motion Control Conference EPE-PEMC 2010*, Sep. 2010. doi: 10.1109/EPEPEMC.2010.5606610.

[17] G. Owusu, J. K. Annan, and S. Nunoo, "Neural network-based optimisation of sinusoidal PWM controller for VSI-driven BLDC motor," *Power Electronics and Drives*, vol. 8, no. 1, pp. 275–298, Jan. 2023, doi: 10.2478/pead-2023-0018.

[18] A. D. Prasad, M. Siva, and A. S. Reddy, "Optimizing slow-charging EV loads with a two-layer strategy to enhance split-phase voltage quality and mitigate issues in PDNs," *International Journal of Power Electronics and Drive Systems*, vol. 16, no. 3, pp. 1472–1483, 2025, doi: 10.11591/ijpeds.v16.i3.pp1472-1483.

[19] M. M. A. Alakkad, Z. Rasin, M. Rasheed, and R. Omar, "Harmonic minimization using artificial neural network technique for CHB-ML inverter," in *2021 IEEE International Conference in Power Engineering Application (ICPEA)*, Mar. 2021, pp. 12–17. doi: 10.1109/ICPEA51500.2021.9417759.

[20] R. Jadeja, A. Ved, and S. Chauhan, "An investigation on the performance of random PWM controlled converters," *Engineering, Technology & Applied Science Research*, vol. 5, no. 6, pp. 876–884, Dec. 2015, doi: 10.48084/etasr.599.

[21] H. M. S. Sajid, M. B. Shafi, N. Malik, A. Muhammad, and A. Amin, "Design of three phase inverter system with LC filter," in *2020 IEEE 23rd International Multitopic Conference (INMIC)*, Nov. 2020, pp. 1–5. doi: 10.1109/INMIC50486.2020.9318075.

[22] N. I. Raju, M. S. Islam, and A. A. Uddin, "Sinusoidal PWM signal generation technique for three phase voltage source inverter with analog circuit & simulation of pwm inverter for standalone load & micro-grid system," *International Journal of Renewable Energy Research*, vol. 3, no. 3, pp. 647–658, 2013, doi: 10.20508/ijrer v3i3.771.g6188.

[23] A. Ali and W. K. Mashwani, "A supervised machine learning algorithms: applications, challenges, and recommendations," *Proceedings of the Pakistan Academy of Sciences: A. Physical and Computational Sciences*, vol. 60, no. 4, Dec. 2023, doi: 10.53560/PPASA(60-4)831.

[24] H. Jamil, F. Qayyum, N. Iqbal, and D.-H. Kim, "Enhanced harmonics reactive power control strategy based on multilevel inverter using ML-FFNN for dynamic power load management in microgrid," *Sensors*, vol. 22, no. 17, p. 6402, Aug. 2022, doi: 10.3390/s22176402.

[25] A. K. Thangapandi, A. Kumar, D. Karthigeyan, S. Ramasamy, V. Arumugam, and G. Gatto, "A novel artificial neural network based selection harmonic reduction technique for single source fed high gain switched capacitor coupled multilevel inverter for renewable energy applications," *Heliyon*, vol. 10, no. 19, 2024, doi: 10.1016/j.heliyon.2024.e38550.
[26] A. R. Singh *et al.*, "AI-enhanced power quality management in distribution systems: implementing a dual-phase UPQC control with adaptive neural networks and optimized PI controllers," *Artificial Intelligence Review*, vol. 57, no. 11, 2024, doi: 10.1007/s10462-024-10959-0.
[27] V. Mohan, G. Krithiga, M. T. Alagan, and V. Sathya, "Sunflower-based butterfly optimization algorithm with enhanced RNN for the harmonics elimination in multilevel inverter," *Discover Applied Sciences*, vol. 7, no. 8, p. 803, Jul. 2025, doi: 10.1007/s42452-025-07475-3.

BIOGRAPHIES OF AUTHORS

Halidu Abdul Mumin received his B.Sc. degree in electrical, electronic, and automation engineering from Université M'hamed Bougara de Boumerdès, Algeria, in 2014, and his M.Sc. degree in power systems and machines in 2016. He is a lecturer in the Department of Electrical and Electronic Engineering, Dr. Hilla Limann Technical University, Wa, Ghana. He is currently pursuing his Ph.D. in electrical engineering at the University of Mines and Technology (UMaT), Tarkwa, Ghana. His research interests include power electronics and drive systems, inverter control technology, pulse width modulation and its optimization, as well as harmonic analysis and mitigation. He can be contacted at email: amhalidu@dhltu.edu.gh.

Solomon Nunoo received the B.Sc. degree in Electrical/Electronic Engineering from Western University College of KNUST, Tarkwa, Ghana, in 2004, the M.Phil. degree in electrical and electronic engineering from UMaT, in 2007, and the Ph.D. degree in electrical engineering from Universiti Teknologi Malaysia (UTM), Johor, Malaysia, in 2015. He is currently an associate professor in the Department of Electrical and Electronic Engineering, UMaT, Tarkwa. His research interests include energy management and statistical signal processing, with emphasis on adaptive filtering, compressive sampling, and wireless communications. He is a member of the IEEE and IAENG. He can be contacted at email: snunoo@umat.edu.gh.

Joseph Cudjoe Attachie is an associate professor in the Department of Electrical and Electronic Engineering, University of Mines and Technology (UMaT), Tarkwa, Ghana. He is currently an associate professor in the Department of Electrical and Electronic Engineering, UMaT, Tarkwa. He holds a Ph.D. degree in electrical engineering from UMaT, Tarkwa, and an M.Sc. degree in electrical engineering from the National Technical University (NTU), Ukraine. He is a member of IAENG and the Ghana Institution of Engineers (GhIE). His research interests include electrical power systems and networks, power quality, high-voltage engineering, and energy management. He can be contacted at email: jcattachie@umat.edu.gh.